SOILS AND FOUNDATIONS

Stability Monitoring of Rainfall Induced Deep Landslides Through Pore Pressure Profile Measurements

--Manuscript Draft--

Manuscript Number:	
Full Title:	Stability Monitoring of Rainfall Induced Deep Landslides Through Pore Pressure Profile Measurements
Article Type:	Technical Paper
Corresponding Author:	Jui-Ting Lee, M.D. National Chiao Tong University , TAIWAN
Corresponding Author Secondary Information:	
Corresponding Author's Institution:	National Chiao Tong University
Corresponding Author's Secondary Institution:	
First Author:	An-Bin Huang, Professor
First Author Secondary Information:	
All Authors:	An-Bin Huang, Professor
	Jui-Ting Lee, M.D.
	Yen-Te Ho, PhD
	Yun-Fang Chiu, PhD
All Authors Secondary Information:	
Abstract:	Due to its geological and meteorological conditions, landslides during typhoon seasons are common in Taiwan. Engineers and government officials are particularly concerned about the potentially deep seated landslides as their scale can be massive and consequences devastating. It has long been recognized that field hydrological and geomechanical properties/conditions are the key elements controlling the stability of a slope under the influence of rainfall. Warning systems based on rainfall or ground displacement measurements are popular methods currently used in minimizing the hazards of landslides. Field hydrological monitoring, when it is used, usually involves limited number of sensors for either positive or negative pore-water pressure measurements. Available numerical schemes that couple pore-water pressure into geomechanical analysis are most suitable for shallow slope failures. Due to the variable and transient nature of hydrological conditions in earth slopes, field measurements that reflect the pore-water pressure profile on a real-time basis would be highly desirable. The authors developed a piezometer system that is based on optical fiber Bragg grating (FBG) pressure sensors. With this system, an array of nine sensors was installed in a single, 60m deep borehole to monitor the pore-water pressure profile at a highway slope in Southern Taiwan. The paper describes the details of FBG sensor array installation in the field and data obtained through three typhoons from 2008 to 2010. The results demonstrated that the field readings can be readily incorporated into the existing mechanics based analytical frameworks and predict the potential of an incoming slope failure.

Stability Monitoring of Rainfall Induced Deep Landslides Through Pore Pressure Profile Measurements

by

1. Prof. An-Bin Huang

Email: abhuang@mail.nctu.edu.tw

Postal Address: Department of Civil Engineering, National Chiao-Tung University, Hsinchu, Taiwan

Phone: +886-722803

Fax: +886-35716257

2. Jui-Ting Lee (corresponding author)

Email: ruiting.cv92g@nctu.edu.tw

Postal Address: Department of Civil Engineering, National Chiao-Tung University, Hsinchu, Taiwan

Phone: +886-35712121 ext. 55009

Fax: +886-35716257

3. Dr. Yen-Te Ho

Email: ytho@mail.nctu.edu.tw

Postal Address: Department of Civil Engineering, National Chiao-Tung University, Hsinchu, Taiwan

Phone: +886-35712121 ext. 55270

Fax: +886-35716257

4. Dr. Yun-Fang Chiu

Email: yfchiu@mail.ihmt.gov.tw

Postal Address: Harbor and Marine Technology Center, Taichung, Taiwan

Phone: +886-426587200

Fax: +886-426571329

Abstract

Due to its geological and meteorological conditions, landslides during typhoon seasons are common in Taiwan. Engineers and government officials are particularly concerned about the potentially deep seated landslides as their scale can be massive and consequences devastating. It has long been recognized that field hydrological and geomechanical properties/conditions are the key elements controlling the stability of a slope under the influence of rainfall. Warning systems based on rainfall or ground displacement measurements are popular methods currently used in minimizing the hazards of landslides. Field hydrological monitoring, when it is used, usually involves limited number of sensors for either positive or negative pore-water pressure measurements. Available numerical schemes that couple pore-water pressure into geomechanical analysis are most suitable for shallow slope failures. Due to the variable and transient nature of hydrological conditions in earth slopes, field measurements that reflect the pore-water pressure profile on a real-time basis would be highly desirable. The authors developed a piezometer system that is based on optical fiber Bragg grating (FBG) pressure sensors. With this system, an array of nine sensors was installed in a single, 60m deep borehole to monitor the pore-water pressure profile at a highway slope in Southern Taiwan. The paper describes the details of FBG sensor array installation in the field and data obtained through three typhoons from 2008 to 2010. The results demonstrated that the field readings can be readily incorporated into the existing mechanics based analytical frameworks and predict the potential of an incoming slope failure.

Key words: Fiber optic sensing, pore-water pressure, landslide, rainfall

Introduction

Rainfall has been considered as one of the most frequent triggering factors to natural slope failures (De Vita and Reichenbach, 1998). The rainfall triggered landslides can cover large areas and they generally involve shallow soil deposit of different grading and origin. Significant and frequent landslides have been reported in Central America, New Zealand, Hong Kong and Japan (Cascini et al., 2010). Considering the destructive nature of landslides, attempts have been made to predict or model the occurrence of rainfall induced slope failures. Keefer et al. (1987) described the implementation of a real-time landslide warning system based primarily on precipitation intensity-duration thresholds developed by Cannon and Ellen (1985), with consideration also given to seasonal antecedent precipitation. The rainfall intensity-duration threshold based methods are empirically developed using previous records for a given region.

It has long been recognized that field hydrological and geomechanical properties/conditions are the key elements controlling the stability of a slope under the influence of rainfall (Johnson and Sitar, 1990; Anderson and Sitar, 1995; Fannin and Jaakkola, 1999; Collins and Znidarcic, 2004; Cascini et al., 2010; Kitamura and Sako, 2010; and Rahardjo et al., 2010). Thus, a mechanics based system that considers the current and local soil/groundwater conditions should be a desirable approach in providing an effective analysis or warning for a potential landslide at a given location.

Significant contributions have been made in analyzing the phenomenon of rainfall induced landslides. This type of landslides are mainly caused by 1) increase of soil unit weight; 2) reduction of suction in unsaturated soil with increasing water content; 3) seepage force resulted from water infiltration; and 4) rise of groundwater table. Collins and Znidarcic

(2004) analyzed shallow landslides with failure planes that have small depth-to-length ratios, as an infinitely long slope failure. It was assumed that each slice of the infinitely long slope was subjected to the same amount and intensity of rainfall. An individual slice was numerically simulated as a one-dimensional soil column subjected to vertical infiltration. For a slope with initial groundwater table below the slope surface, soil above the groundwater table is unsaturated with negative pore water pressure or suction. Soil becomes more saturated as the infiltration progresses downward. The hydraulic conductivity typically increases with increasing water content when soil is unsaturated. As the soil becomes saturated, the hydraulic conductivity reaches a maximum and constant value. Water infiltration saturates the soil column over time beginning from the initial hydrostatic suction profile. The one-dimensional numerical seepage analysis considers these unsaturated soil characteristics and computes the transient capillary and pore-water pressure head (h_c and h_p, respectively) profiles in response to rainfall water infiltration. The fine grain soil conducts water more freely through its channel network so that the resistance to flow is minimized and pressure head in excess of the steady state value does not arise. With fewer pores initially filled with water in unsaturated coarse grain soil, there are fewer channels available for fluid transport and consequently the flow of water is hindered. Thus, less negative or even positive pressure heads are more likely to develop in coarse than in fine grain soil as a result of downward infiltration. Positive pore water pressure development is a consequence of the need to “push” water into unsaturated soil with lower permeability. The development of the positive pore pressure is analogous to the establishment of a perched water table in the upper part of the layer. Such high gradients are absent from the infiltration profiles for fine-grained soils since the hydraulic conductivity changes more gradually.

Considering the equilibrium of gravity, available soil resistance and seepage forces imposing on the slice, a relationship among the critical depth for infinite slope failure (d_{cr}), soil strength parameters and pore-water pressure head was established as,

$$d_{cr} = \frac{c' + \gamma_w \cdot h_c \cdot \tan\phi^b - \gamma_w \cdot h_p \cdot \tan\phi'}{\gamma \cdot \cos^2\beta \cdot (\tan\beta - \tan\phi')} \tag{1}$$

where

β = slope angle

c' = drained cohesion

γ = saturated unit weight of soil

γ_w = unit weight of water

ϕ' = drained friction angle

ϕ^b = friction angle with respect to matric suction (= γ_w h_c)

In unsaturated soil $h_p = 0$, when soil becomes saturated, $h_c = 0$. According to Equation (1), for slope angles less than friction angle ($\beta < \phi'$), failure in the unsaturated soil layer is not possible. In the case of $\beta > \phi'$, slope can fail when soil is still unsaturated with negative pore water pressure. The coupling of Equation (1) and one-dimensional seepage analysis enables quantitative predictions about the time and depth of a shallow slope failure. Figures 1 and 2 show the evolution of pressure head profiles (h_c or h_p versus depth of infiltration) as infiltration progresses in a rainfall event, in the case of $\beta > \phi'$ and $\beta < \phi'$, respectively. Slope failure occurs at depth d_{cr} where the pressure head profile touches the stability envelope. The stability envelope is a graphic presentation of Equation (1). Cascini et al. (2010) described a system that divided a landslide into failure, postfailure and propagation stages, according to their distinct kinematic characteristics. Failure and postfailure stages occur inside the landslide source areas. Failure stage is characterized by the formation of a continuous shear surface through the soil mass. Postfailure stage is represented by the rapid generation of large plastic strains and the consequent sudden acceleration of the failed soil mass. Propagation stage includes movement of the failed soil mass from the landslide source areas to the deposition areas, where the failed soil mass stops. Figure 3 shows a field stress path based scheme reported by Cascini et al. (2010) to conceptually describe the characteristics of failure and postfailure stages that involve infiltration from the surface and spring from the bedrock. The same figure also describes qualitatively the change in ground displacement (δ), resisting force (F_r) and driving force (F_d) imposing on the failed soil mass with time, t. For given strength parameters or the failure envelope of the slope soil, the initial effective stress point (p', q) of the soil within a stable slope are located to the right side of the failure envelope (at point 0) as shown in Figure 3. The definition of p' and q are:

$$p' = (\sigma_1' + \sigma_2' + \sigma_3')/3 \tag{2}$$

$$q = \frac{1}{\sqrt{2}}\sqrt{(\sigma_1' - \sigma_3')^2 + (\sigma_1' - \sigma_2')^2 + (\sigma_2' - \sigma_3')^2} \tag{3}$$

where

σ_1', σ_2', and σ_3' = major, intermediate and minor principal stress, respectively

The postfailure stage refers to the characteristics of the slope failure after the stress point reaches the failure envelope.

For the cases of Figures 3(b) and 3(d), the external loading condition or driving force (F_d) remains constant, the hydrologic response of the slope (i.e., surface infiltration and spring) causes the pore water pressure to increase and the effective stress point to move horizontally towards the failure envelope. The increase of pore water pressure reduces resisting force, F_r and ground displacement, δ develops as the stress point moves from 0 to 1. The slope failure initiates when the stress point reaches the failure envelope at point 1 and $F_r = F_d$. If the soil remains drained (no increase in pore water pressure) following the slope failure, the slope failure is referred to as slide. The failed soil mass experience low acceleration, a and there is no significant increase in δ when $t > t_1$. If the pore water pressure accumulates due to contractive behavior of the slope soil and/or poor drainage conditions, flowslide develops (Figure 3(c)). In this case the stress point moves towards the origin along the failure envelope, large acceleration develops ($a >> 0$) and δ increases significantly while F_r further decreases when $t > t_1$. Figure 3(d) shows a case of slide to flow that involves the increase of F_d in the failure stage. Following point 1 the stress point moves vertically towards the failure envelope until failure at point 2. The postfailure stage associates with high acceleration and displacement when $t > t_2$ as in the case of flowslide. The increase in F_d can be due to unbalanced driving forces from upslope failure. Excluding the case of slide to flow, the failure onset of rainfall induced shallow landslides can be considered as strictly related to the increase of pore-water pressures (Anderson and Sitar 1995; Leroueil, 2001; and Take et al. 2004). Notwithstanding our understanding of the importance of pore water pressure, ground displacement measurements using the inclinometer casing is still the most popular method for slope stability monitoring. As qualitatively described in Figure 3, δ steadily and gradually increases as the stress point moves towards the failure envelope. However, it is difficult to establish a relationship between δ and proximity of slope soil failure (i.e., proximity between the stress point and failure envelope). Theoretically, it is possible to identify the onset of a slope failure when the rate of δ increases significantly when $t > t_2$ in Figure 3(c) or $t > t_1$ in Figure 3(d), but the slope has failed (i.e., the stress point has reached the failure envelope) by then. Pore-water pressure is probably the most indicative of slope instability in its early stage, among the viable physical quantities that can be monitored in the field. Monitoring of positive and negative pore pressures using piezometers and tensiometers, respectively, has been reported for slopes in different parts of the world (Cowland and Richards, 1985; Johnson and Sitar, 1990; Fannin and Jaakkola, 1999; Ng et al., 2003; Zhan et al., 2007; and Ng et al., 2008). A tensiometer is usually inserted into the shallow ground directly for measurement of negative pore pressure at a single depth. The current practice in groundwater level or positive pore-water pressure monitoring generally involves the installation of one or two open end piezometers (i.e., standpipe), pneumatic or electric pressure transducers in a typical 100mm diameter borehole. Fannin and Jaakkola (1999) reported from their experience that the field pore pressure measurements rarely showed a linear distribution with depth or a uniform response across the slope. Soil stratification, subsurface conduits such as soil pipes or animal burrows create highly permeable drainage paths (Johnson and Sitar, 1990; Fannin and Jaakkola, 1999). When blocked, these conditions can create instant pore pressure buildup. Sidle (1984) has also indicated that pore pressure buildup can be quite rapid, can vary in character along the slope, and cannot be entirely explained by assuming only vertical infiltration through soil.

Due to its geological and meteorological conditions, landslides during typhoon seasons are common in Taiwan. A relatively deep and massive landslide occurred above Shiaolin Village of Kaohsiung County in Taiwan during typhoon Morakot of 2009. The debris buried and killed 500 local residents. The slope angle before failure was less than 23°; failure surface was approximately 84m deep. Deep seated slope failures are relatively rare, but its consequences can be devastating. An effective landslide warning system would be very useful in mitigating the hazards of such deep seated and potentially massive landslides.

The above described literature often referred to their analyses as “shallow” slope failures, with depth of shear planes generally less than 5m. For deep seated landslides, direct measurement of pore water pressure profile on a real-time basis would be desirable. The field monitoring should be automated and with sufficient measurement points to reveal the highly non-linear and transient pore-water pressure profiles resulted from heavy rainfall. There are commercially available vibrating wire (VW) piezometers that allow multiple units to be connected in a series and installed in a single borehole. The electric sensors such as the VW piezometers can be affected by electromagnetic interference, lightning and/or short circuit when placed under water, in the field. Little has been reported on long term, automated pore-water pressure profile monitoring using an array of VW type of piezometers.

Fiber Bragg Grating (FBG) is a partially distributive optical fiber sensor where signal is transmitted via light. Multiple FBG sensors can be connected to a single, 250μm diameter optical fiber. The FBG optical signal can easily be transmitted over 10km in distance and is immune to electromagnetic interference, short circuit or lightning. The stability of optical fiber is not significantly affected by submergence under water. These unique features make FBG sensors ideally suited for the purpose of monitoring ground conditions where a profile-information is required. The authors have developed an FBG piezometer based on the technique reported by Ho et al. (2008). An array of FBG piezometers can be installed in a single borehole to monitor the profile of pore-water pressure on a real-time basis. When coupled with the limiting equilibrium or field stress path framework as described above, it is possible to establish a landslide warning system based on field h_p profile measurements on a real-time basis.

Field installation of an FBG piezometer array was experimented at a highway slope of Alishan Mountain in Southern Taiwan. This paper describes the techniques of FBG pressure sensing and installing FBG piezometer array in a single borehole that was 60m deep. The h_p profiles recorded during three major typhoons in 2008-2010, slope stability analysis using the infinite slope, field stress path and limiting equilibrium frameworks based on the field h_p data and implications in future applications as part of a landslide warning system are presented and discussed.

Partially Distributive FBG Piezometers

A fiber Bragg grating (FBG) is made by periodic variation of the core refractive index on a 1 to 20 mm long segment of optical fiber (Meltz et al., 1989). When the FBG is illuminated by a wideband light source, a fraction of the light is reflected back upon interference by the FBG. The wavelength of the reflected light is linearly related to the longitudinal strains of the FBG. Thus, FBG has the same function as a strain gage. The returned signal from every FBG carries a unique range or domain of wavelength, making it possible to have multiple FBG elements on the same fiber. The multiplexing among various sensors on a single optical fiber can be accomplished by wavelength division addressing as conceptually described in Figure 4. There is a limited bandwidth of the light source and as the light passes an FBG there is a loss of its intensity, the number of FBG sensors that can be placed on a fiber is not more than 20 with the currently available FBG interrogation systems.

Figure 5 shows a schematic view and photograph of an FBG pressure transducer. The FBG was used to sense the deflection of a metallic diaphragm inside of the transducer due to changes in pressure against the atmosphere. A separate FBG was placed inside the transducer to monitor temperature fluctuations. A typical interrogation system is capable to detect shifting of FBG wavelength by 1pm (10^{-12} m). An FBG breaks when stretched by a strain equivalent to approximately 8000 to 10000pm in wavelength variation. The range of pressure transducer was controlled by the stiffness of the diaphragm. Depending on the required safety margin, the maximum allowable pressure was designed to correspond to 1000 to 6000pm of FBG wavelength variation.

The pressure transducer was converted into a piezometer by surrounding the drains with filter material. With a diameter of 25mm, the FBG piezometer was fitted inside of a 28mm ID and 32mm OD PVC pipe. Small drainage holes were drilled in the PVC pipe in areas surrounding the piezometer to allow passage of water. The piezometer was epoxied and sealed at both ends in the PVC pipe to prevent seepage between piezometers from within the PVC pipe. The PVC pipe serves as a spacer and housing for the piezometers and optical fiber. All PVC pipe connectors were internal leaving a smooth exterior upon assembly in the field. The assembled PVC pipe/piezometers can be fully grouted in a borehole following the procedure reported by Contreras et al. (2008). Or, the piezometers can be surrounded by a sand pack and the space between sand packs sealed with bentonite. A comparison between an array of FBG piezometers installed in a single borehole to the case of individual, separate installation of standpipes is depicted in Figure 6.

Field Installation at Five Turn Point

A section of Highway 18 that connects Chiayi County to Alishan Mountain, referred to as the Five Turn Point has been selected as the most dangerous highway in Taiwan. The Five Turn Point is located in a slope area of approximately 1200m by 1000m where the ground surface elevation changed by as much as 400m. Alishan is a major mountain resort in Southern Taiwan that attracts large number of tourists in the summer which is also the typhoon season. Figure 7 shows a topographic map of the general area of Five Turn Point. The highway in this section originally had five turns in order to increase the linear dimension and maintain a desirable grade for the vehicles. At least eight sectors (designated as N1 to N8 in Figure 7) within the Five Turn Point area have been identified with either previous slope failure or signs of continuous movement. The shear planes could reach as much as 80m below ground surface. The most recent massive landslide occurred in N4 on June 26, 2003. The slope failure and rerouting of the highway created additional turns. Figure 8 depicts cross sectional view of section B-B that has an average slope angle of 23°. The shear planes associated with earlier ground failures according to available investigations are also included in Figure 8. Previous subsurface explorations revealed that the subject area was covered by 0-26m of colluvial material that consisted of a mixture of soil and rock pieces. Interlayered sandstone and shale extended from below the colluvial to over 200m (deepest bore hole available) below the ground surface. Affected by numerous folding and fault movements, the rock formation was severely fractured with no consistent joint pattern. The rock quality designator (RQD) obtained from rock coring ranged from below 5 to over 50 with no consistent trend with depth. The random RQD values were observed even in boreholes as deep as 200m. Because of the wide range in sizes of the fractured rock pieces, it was not possible to obtain good quality samples for laboratory shearing tests and to provide representative strength parameters. Open end piezometers or standpipes with the measuring tip at 50-80m below ground surface have been used to monitor the ground water table. The groundwater could rise from its low level by more than 20m as a result of heavy rainfalls according to available data shown in Figure 8. The sudden and significant change in groundwater table is believed to be a major cause for the earlier slope failures in this area.

A 60m deep borehole marked as NCTU-03 in Figures 7 and 8 was used to install the FBG piezometer array. The FBG piezometer was housed in PVC pipes as describe above. Additional PVC pipe was connected in the field to space the FBG piezometers at 5m intervals. The segment of the PVC pipe that contained the FBG piezometer was wrapped with 1.5m wide non-woven geotextile outside the PVC pipe as filter. Figure 9 shows a set of PVC pipes with FBG piezometers enclosed. The optical fibers were threaded through the inside of the PVC pipes. Final assembly was made as the PVC pipe lowered into the borehole. The borehole had a nominal diameter of 150mm (6 inch). A steel casing of 100mm inside diameter was extended to the bottom of the borehole before piezometer installation. The FBG piezometer array was fully assembled and inserted into the borehole with the protection of the steel casing. The steel casing was then lifted upward 5m at a time, leaving 5m of the FBG piezometer array/PVC pipe exposed to the surrounding material. The FBG piezometer was surrounded by 2m thick sand pack (see Figure 6). Sealing between the sand pack was provided by placing bentonite pellets. Sand and bentonite pellets were pumped by water to the desired depth in the borehole using a 32mm OD PVC pipe as a tremie pipe. The deepest piezometer was located at 59m below ground surface. The sensors were connected to an on-site computer using optical fiber cables for optical signal interrogation and data logging. The field computer was accessed via High-Speed Downlink Packet Access (HSDPA) wireless internet system. The readings were updated hourly.

Field Measurements through Three Typhoons

The FBG piezometer installation at Five Turn Point was completed in mid-October, 2007. Figure 10 shows a set of representative readings taken between October 26, 2007 (beginning of automated data logging) and August 31, 2008. The piezometer at 59m malfunctioned from the beginning. The initial readings reflected a groundwater table at 40m below ground surface. The water table remained low for the most part of the monitored period in Figure 10 except for those of 6/11 and 7/22 of 2008, when a mild rain storm occurred. A perched water table at 24m developed after April 14, 2007. Negative pore-water pressure was registered at 14m below ground surface in the early stage of monitoring.

The Five Turn Point slope endured three major typhoons since September 2008, and remained stable till now (December, 2011). Typhoon Sinlaku landed in Southern Taiwan on September 14, 2008 and brought in rainfall that peaked at 660mm/day with an accumulated value approaching 1000mm. A histogram of daily precipitations during the period that includes typhoon Sinlaku is shown in Figure 11. The rain gauge with its location marked in Figure 7, was located within 100m from the piezometer borehole (NCTU-03 of Figures 7 and 8). Figure 12 shows a set of representative h_p profiles based on the FBG piezometer readings recorded from the beginning of typhoon Sinlaku to the time when h_p reached the maximum measurement values. The rainfall intensity peaked on September 14, while the maximum h_p profile was recorded on September 15 with a one-day lagging. The presentation of h_p profiles followed the same infinite slope framework as in Figure 2, except that the h_p values were taken from field measurements rather than one-dimensional seepage analysis. The stability envelopes included in Figure 12 was determined using Equation (1). The highly fractured rock pieces were considered as coarse granular material. The analysis considered the cross section shown in Figure 8, with a slope angle (β) of 23° and the selected ϕ' values while ϕ^b and c' were assumed to be 0, and $\gamma = 2\,\gamma_w$. The h_p profiles showed significant development of a perched water table at 24m below ground surface. This phenomenon is believed to be caused by the decrease of hydraulic conductivity at the interface where the ground material changed from saturated to unsaturated state when water seeped into the ground, as described by Collins and Znidarcic (2004) for slopes with coarse material. Figure 12 also demonstrates that if the ground material had a ϕ' less than 36°, the slope would have failed with shear planes developed at 24 and 54m below ground surface.

The pore-water pressure readings also enabled the concept of field stress path (Anderson and Sitar, 1995; and Cascini et al., 2010) to be used in evaluating the stability of the slope. The initial state of stress at each of the pore-water pressure measurement locations was computed using the commercial software SIGMA/W (GEO-SLOPE International Ltd., 2007). The computation was based on the cross section shown in Figure 8. The ground material was assumed to be linear elastic with Young's modulus E = 3310MPa, Poisson's ratio $\mu = 0.35$, and $\gamma = 2\,\gamma_w$. For simplification, the single γ value used in the computation reflects a saturated state even when the material could be unsaturated. The potential error from the simplification of unit weight and stress-strain relationship is insignificant in comparison with the stress level and the effects of pore-water pressure variations (Anderson and Sitar, 1995). Considering a plane strain condition, the p (or p') and q were calculated according to Equations (2) and (3), respectively. As the measured pore-water pressure increases, q at a given measurement point remained constant while p' decreases and the corresponding stress point (p', q) moves laterally towards a failure envelope as shown in Figure 13. The (p', q) points depicted in Figure 13 correspond to the respective nine FBG piezometer locations installed in the field. The lower left (p', q) points represent the state of field stress at shallower depths. The results also show a potential failure envelope that corresponds to a ϕ' close to 36°. The advantage of field stress path approach is that it is not necessary to simplify the slope as infinitely long as in the analysis by Collins and Znidarcic (2004). Although not necessary for the Five Turn Point case, variations in slope angle and ground layers can be readily incorporated in the analysis under the framework of field stress path. It should be noted that the outcome of the linear elastic stress analysis was not sensitive to the selection of Young's modulus. However, the selection of Poisson's ratio could have significant effects on the initial p, q values.

Typhoon Morakot landed in Southern Taiwan on August 8, 2009. The histogram of daily precipitations during typhoon Morakot as shown in Figure 14 reflects an accumulated rainfall close to 3000mm. This is more than the average annual rainfall of 2500mm in Taiwan. Rainfall with intensity exceeding 700mm/day continued through August 9, 2009. Unlike typhoon Sinlaku, the pore-water pressure did not show a delayed development, the peak measurement values were reached soon after the rainfall started fading on August 9. Most significant pore water pressure increase occurred in depths between 30 and 50m. The intense rainfall also believed to have induced a perched water table at 24m below ground surface as in the case of typhoon Sinlaku. Using the same slope angle, material properties and the stability envelope as shown in Figure 12 for typhoon Sinlaku, slope failure could be predicted if the ground material had a ϕ' less than 40°, with shear planes at 24 and 54m below ground surface as demonstrated in Figure 15.

The evolution of field stress paths for the case of typhoon Morakot are shown in Figure 16. Consistent with the infinite slope approach, the field stress path analysis also indicated stress points touching the failure envelope that corresponds to ϕ' of 40°.

The rainfall during typhoon Fanapi concentrated mainly on September 19, 2010 as shown in Figure 17. With a total amount less than 300mm, the rainfall was relatively mild. There was no clear sign of a perched ground water at shallow depth. Most of the pore water pressure increase during typhoon Fanapi occurred in depths between 40 and 50m. Unlike the past two typhoons, the relatively high pressure head at the depth of 54m was high before the typhoon and continued to increase towards the end of typhoon as described in Figure 18. This early and significant development of pressure head at 54m may be associated with the influx of spring water as shown in Figure 3 or seepage from upper parts of the slope. Because of this initial condition, the slope was in a more critical condition than the time of typhoon Sinlaku that had a much more intensive rainfall. Both the infinite slope (Figure 18) and field stress path (Figure 19) approaches indicated it would require a ϕ' of more than 36° to maintain the slope stability. Regardless of the rainfall characteristics during the typhoons reported above, none of the field measurements reflected a pore-water pressure profile that is similar to hydrostatic.

A series of slope stability analysis was also performed for the same cross section shown in Figure 8 using the conventional method of slices. The analysis was conducted using the commercial software SLOPE/W (GEO-SLOPE International Ltd., 2007a), considering circular failure surfaces under the Bishop method. The pore-water pressure head profile taken from the peak values in each of the three typhoons were used. These values are shown in Table 1, linear interpolation was used for pore-water pressure between piezometers. The analysis assumes the same pore-water pressure variation with depth for the entire slope. The factors of safety reported in Table 2 from the method of slices are generally lower, but show similar trend with those from the infinitely long slope and field stress path methods.

Concluding Remarks

The FBG piezometer array installed at Five Turn Point over four years ago continued to work today (December, 2011). Nine piezometers spaced at 5m intervals, were installed in a single borehole with depths ranging from 14 to 54m below ground surface. The system performed well through three major typhoons during this period. The stability and durability are mainly due to the unique properties of the optical FBG sensing systems. The experience shows that with the help of partially distributive sensors, field pore-water pressure profile monitoring can be practically implemented. Based on the data collected through three typhoons, the following conclusions can be drawn:

- The pore-water pressure readings obtained at the test site before or during a typhoon deviate significantly from a linear hydrostatic distribution. To properly reflect the hydrological conditions, it is imperative to measure the pore-water pressure profile, especially in the case of a potentially deep seated slope failure.
- Depending on the nature of rainfall pattern and ground water flow, the built-up of

pore-water pressure may show different characteristics. The local rainfall may not be the major factor in controlling the stability of a slope.

- Coupling automated pore-water pressure profile measurements with the infinite slope or field stress path concept, it is feasible to establish a real-time slope failure warning system that is based on the proximity between stress state and a stability envelope. This mechanics based warning system should be preferable to the empirical methods that use ground displacement measurements or rainfall as the key parameter.

FBG piezometer array enables pore-water pressure profile measurements to be made at a selected location, along the borehole direction. The monitoring may not be effective, unless the selected location represents the most critical position in a slope. Also, the friction angles used in the paper were selected rather than measured. An effective scheme to determine the strength parameters for deep seated fractured rock pieces or earth material that involve large particle sizes is necessary to establish a priori failure envelope as part of the landslide warning system.

References

Anderson, S.A., and Sitar, N., 1995, "Analysis of rainfall-induced debris flows," Journal of Geotechnical Engineering, ASCE, Vol.121, No.7, pp.544-552.

Cannon, S.J., and Ellen, S.D., 1985, "Rainfall conditions for abundant debris avalanches, San Francisco Bay region, California. California Geology, Vol.38, No.12, pp.267-272.

Cascini, L., Cuomo, S., Pastor, M., and Sorbino, G., 2010, "Modeling of Rainfall-Induced Shallow Landslides of the Flow-Type," Journal of Geotechnical and Geoenvironmental Engineering, Vol. 136, No. 1, pp.85-98.

Cowland, J.W., and Richards, L.R., 1985, "Transient groundwater rises in sheeting joints in a

Hong Kong granite slope," Hong Kong Engineer, pp.27-32.

Collins, B.D., and Znidarcic, D., 2004, "Stability analyses of rainfall induced landslides." Journal of Geotechnical and Geoenvironmental Engineering, Vol.130, No.4, pp.362-372.

Contreras, I.A., Grosser, A.T. and Ver Strate, R.H. 2008, "The use of the fully grouted method for piezometer installation." Geotechnical Instrumentation News, Vol.26 (June), pp.30-37.

De Vita, P., and Reichenbach, P., 1998, "Rainfall-triggered landslides: A reference list," Environmental Geology, Vol.35, No.2-3, pp.219-233.

Fannin,R.J., and Jaakkola, J., 1999, "Hydrological response of hillslope soils above a debris-slide headscarp," Canadian Geotechnical Journal, Vol.36, pp.1111-1122.

GEO-SLOPE International Ltd., 2007. "SIGMA/W for stress-deformation." Version 7.17, User's guide, Geoslope Int. Lad., Calgary, Alta., Canada.

GEO-SLOPE International Ltd., 2007a. "SLOPE/W for slope analysis." Version 7.17, User's guide, Geoslope Int. Lad., Calgary, Alta., Canada.

Ho, Y.T., Huang, A.B., and Lee, J.T. 2008, "Development of a chirped/differential optical fiber Bragg grating pressure sensor." Journal of Measurement Science and Technology(19):6pp, doi:10.1088/0957-0233/19/4/045304.

Johnson, K.A., and Sitar, N., 1990, "Hydrologic conditions leading to debris-flow initiation," Canadian Geotechnical Journal, Vol.27, pp.789-801.

Keefer, D.K., Wilson, R.C., Mark, R.K., Brabb, E.E., Brown, W.M., Ellen, S.D., Harp, E.L., Wieczorek, G.F., Alger, C.S., and Zatkih, R.S., 1987, "Real-time landslide warning during heavy rainfall," Science, Vol. 238, pp.921-925.

Kersey, A.D. 1992, "Multiplexed Fiber Optic Sensors." Fiber Optic Sensors, Proceedings of SPIE, Vol. CR44, pp.200-225.

Kitamura, R., and Sako, K., 2010, "Contribution of "Soil and Foundations" to studies on rainfall-induced slope failures," Soil and Foundations, Vol. 50m, No.6, pp.955-964.

Land Engineering Consultants, Co., Ltd. 2007, "Highway 28.9K~31.5K（Five Turn Point）landslide investigation, remediation planning and safety evaluation, 3rd overall report." Department of Highway Maintenance, Section V (in Chinese).

Leroueil, S. 2001, "Natural slopes and cuts: movement and failure mechanisms." Geotechnique, Vol.51, No.3, pp.197-243.

Meltz, G., Morey, W.W., and Glenn, W.H. 1989, "Formation of Bragg Gratings in Optical Fibers by a Transverse Holographic Methods." Optics Letters. Vol. 14, pp.283.

Ng, C.W.W., Wang, B. and Tung, Y.K. 2001," Three-dimensional numerical investigations of groundwater responses in an unsaturated slope subjected to various rainfall patterns." Canadian Geotechnical Journal, Vol.38, pp.1049-1062.

Ng, C.W.W., Zhan, L.T., Bao, C.G., Fredlund, D.G., and Gong, B.W. 2003, " Performance of an unsaturated expansive soil slope subjected to artificial rainfall infiltration." Géotechnique, Vol.53, No.2, pp.143-157.

Ng, C.W.W., Springman, S.M., and Alonso, E.E., 2008, "Monitoring the Performance of Unsaturated Soil Slopes," Geotechnical and Geological Engineering, Vol.26, No.6, pp.799-816.

Rahardjo, H., Nio, A.S., Leong, E.C., and Ng Yew Song, N.Y., 2010, "Effects of groundwater table position and soil properties on stability of slope during rainfall," Journal of Geotechnical and Geoenvironmental Engineering, Vol.136, No.11, pp.1555-1564.

Sidle, R.C., 1984, "Shallow groundwater fluctuations in unstable hillslopes of Coastal Alaska," Zeitschrift für Gletscherkunde und Glazialgeologie, Vol.20, pp.79-95.

Take, W. A., Bolton, M. D., Wong, P. C. P., and Yeung, F. J. 2004, "Evaluation of landslide triggering mechanisms in model fill slopes." Landslides, 1, pp.173-184.

Zhan, L.T., Ng, C.W.W., and Fredlund, D.G., 2007, "Field study of rainfall infiltration into a grassed unsaturated expansive soil slope," Canadian Geotechnical Journal, Vol. 44, pp.392-408.

Figure Captions

Figure 1. Infiltration results for the case of $\beta > \phi'$ or fine grain soil with superimposed stability envelope (after Collins and Znidarcic, 2004).

Figure 2. Infiltration results for the case of $\beta < \phi'$ or coarse grain soil with superimposed stability envelope (after Collins and Znidarcic, 2004).

Figure 3. Reference schemes for shallow landslides induced by rainfall directly infiltrating. the slope surface and spring from the bedrock (after Cascini et al., 2010).

Figure 4. FBG sensor array (after Kersey, 1992).

Figure 5. The FBG pressure transducer.

Figure 6. Comparison between the individual separate and piezometer array installations.

Figure 7. Topographic map of the Five Turn Point (after Land Engineering Consultants, Co., Ltd., 2007).

Figure 8. Section B-B of the Five Turn Point (after Land Engineering Consultants, Co., Ltd., 2007).

Figure 9. PVC pipes and those with FBG piezometers enclosed.

Figure 10. Piezometer record up to 8/31/2008.

Figure 11. Rainfall record during typhoon Sinlaku.

Figure 12. Profiles of hp during typhoon Sinlaku.

Figure 13. Evolution of field stress paths during typhoon Sinlaku.

Figure 14. Rainfall record during typhoon Morakot.

Figure 15. Profile of hp during typhoon Morakot.

Figure 16. Evolution of field stress paths during typhoon Morakot.

Figure 17. Rainfall record during typhoon Fanapi.

Figure 18. Profiles of hp during typhoon Fanapi.

Figure 19. Evolution of field stress paths during typhoon Fanapi.

Table Captions

Table 1. Pressure head profiles used in method of slice analysis.

Table 2. Factors of safety from the analysis using the method of slices.

Figure1
Click here to download high resolution image

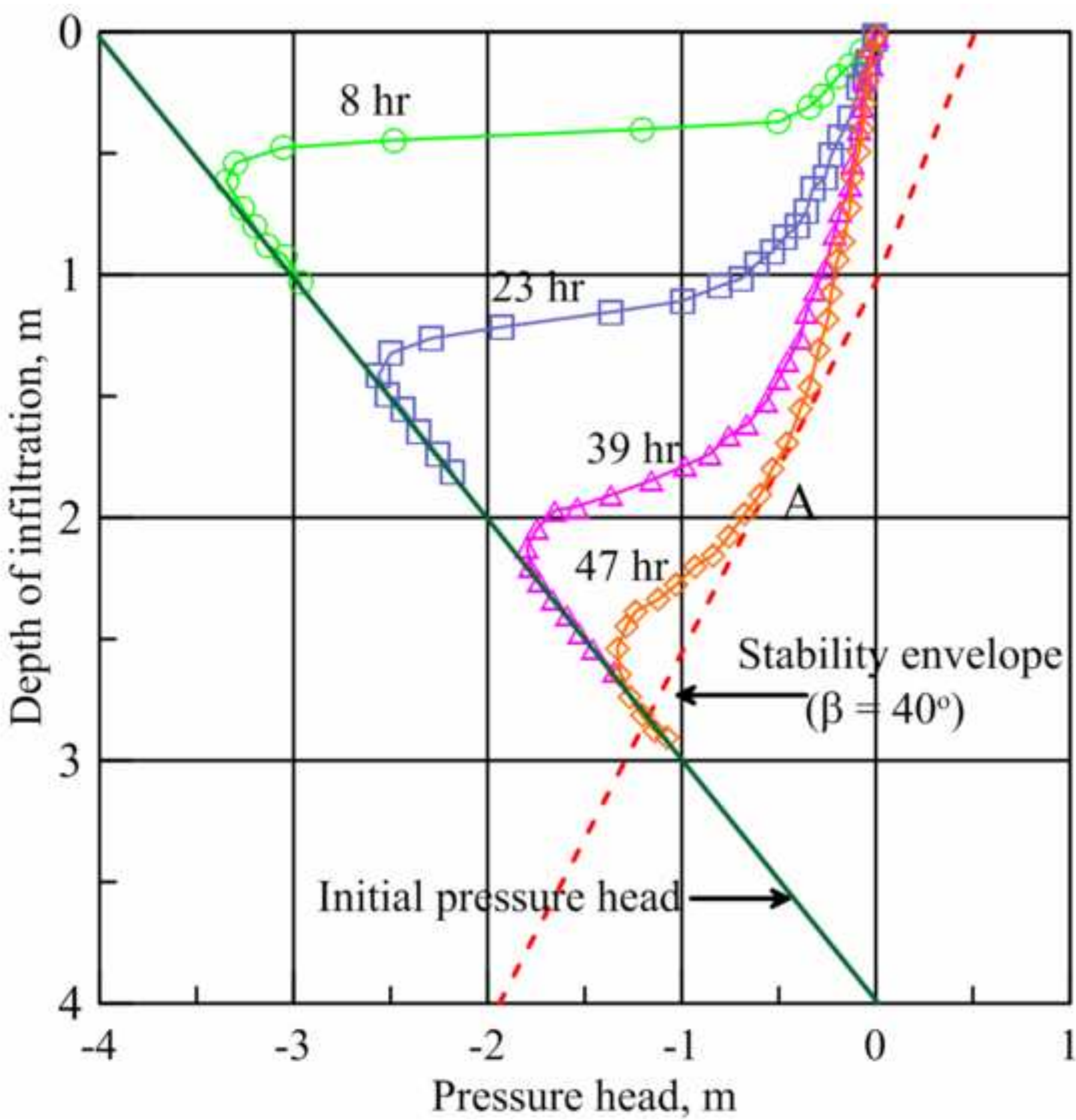

Figure2
Click here to download high resolution image

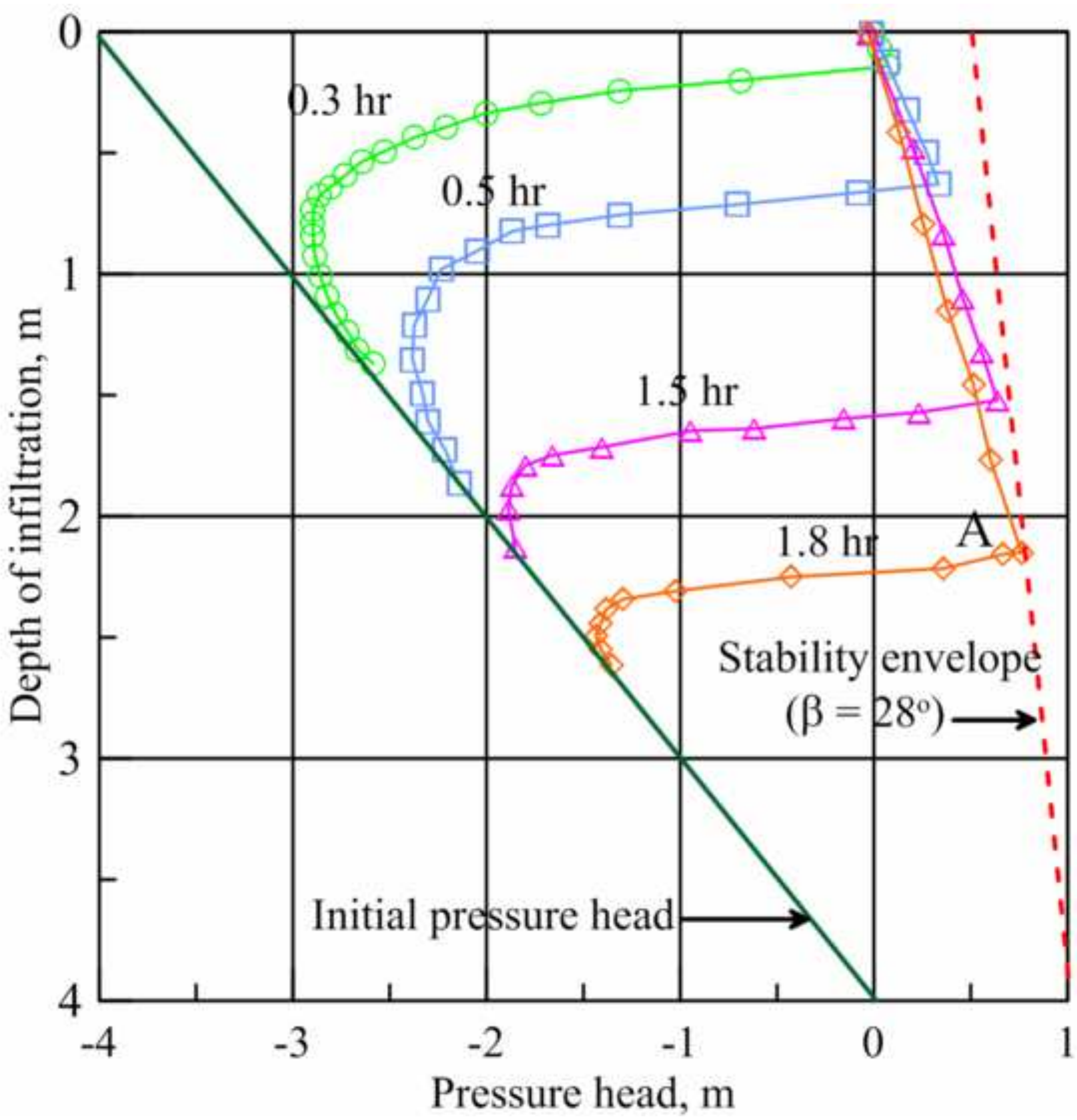

Figure3

Click here to download high resolution image

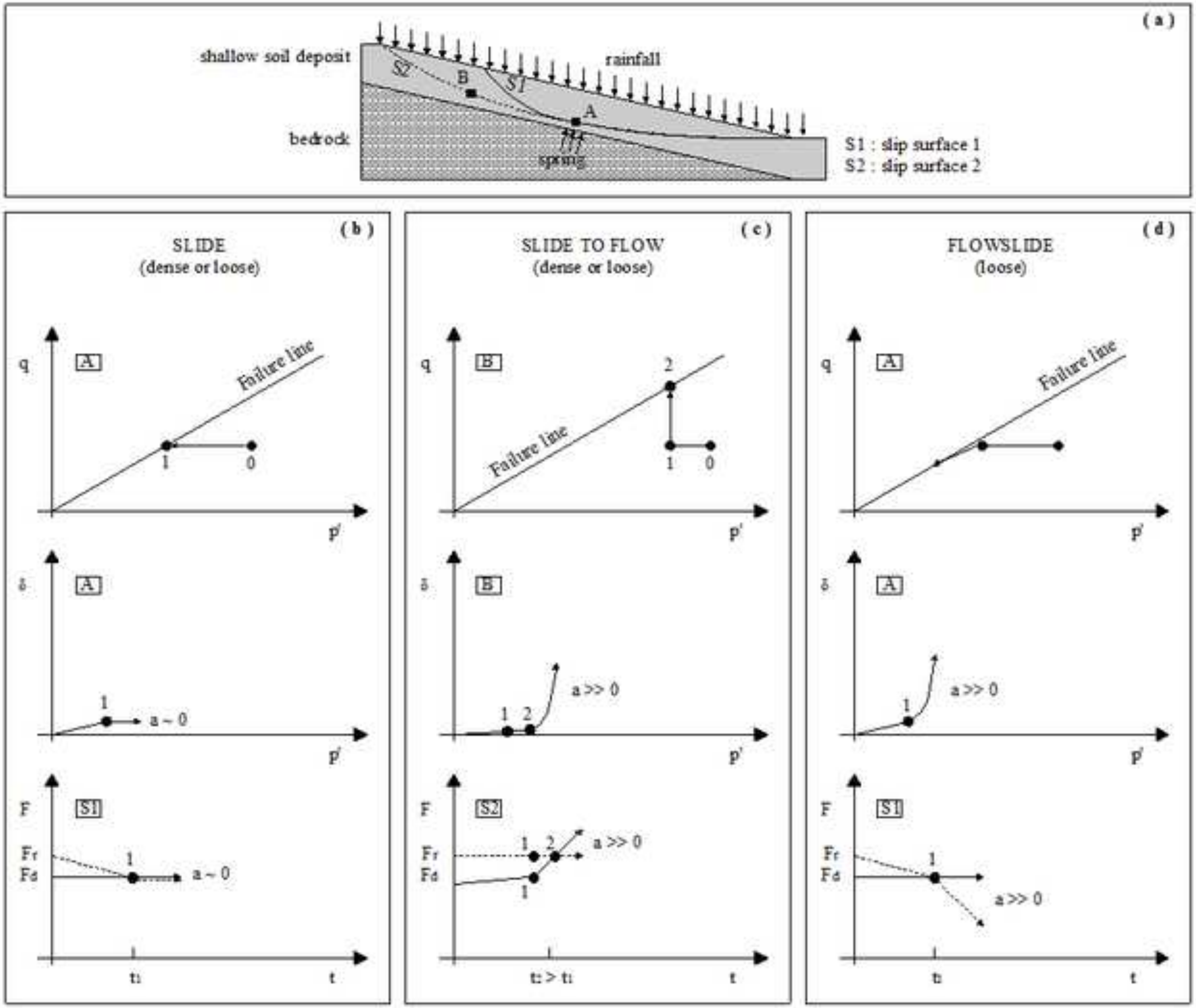

Figure4
Click here to download high resolution image

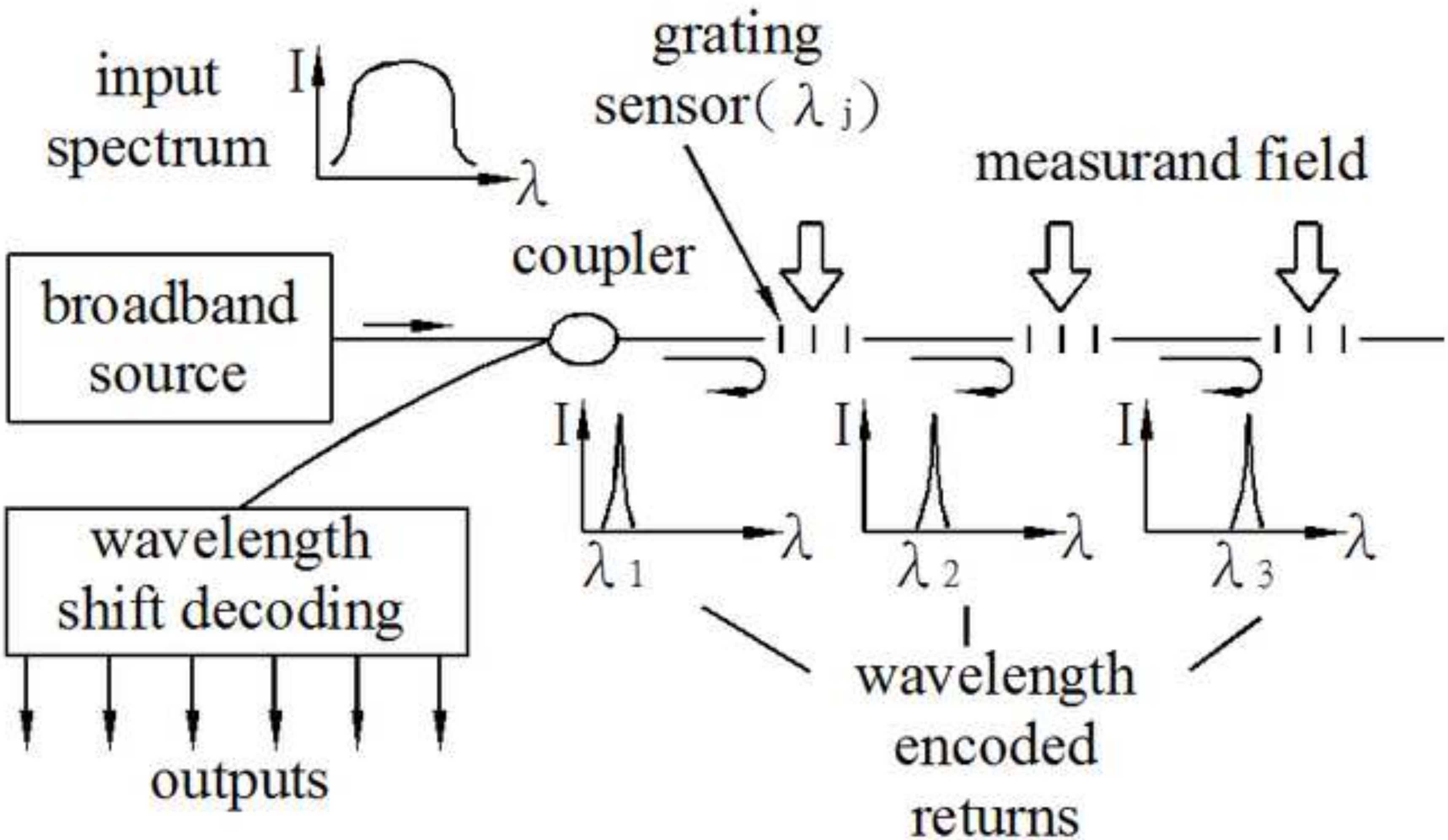

Figure5

Click here to download high resolution image

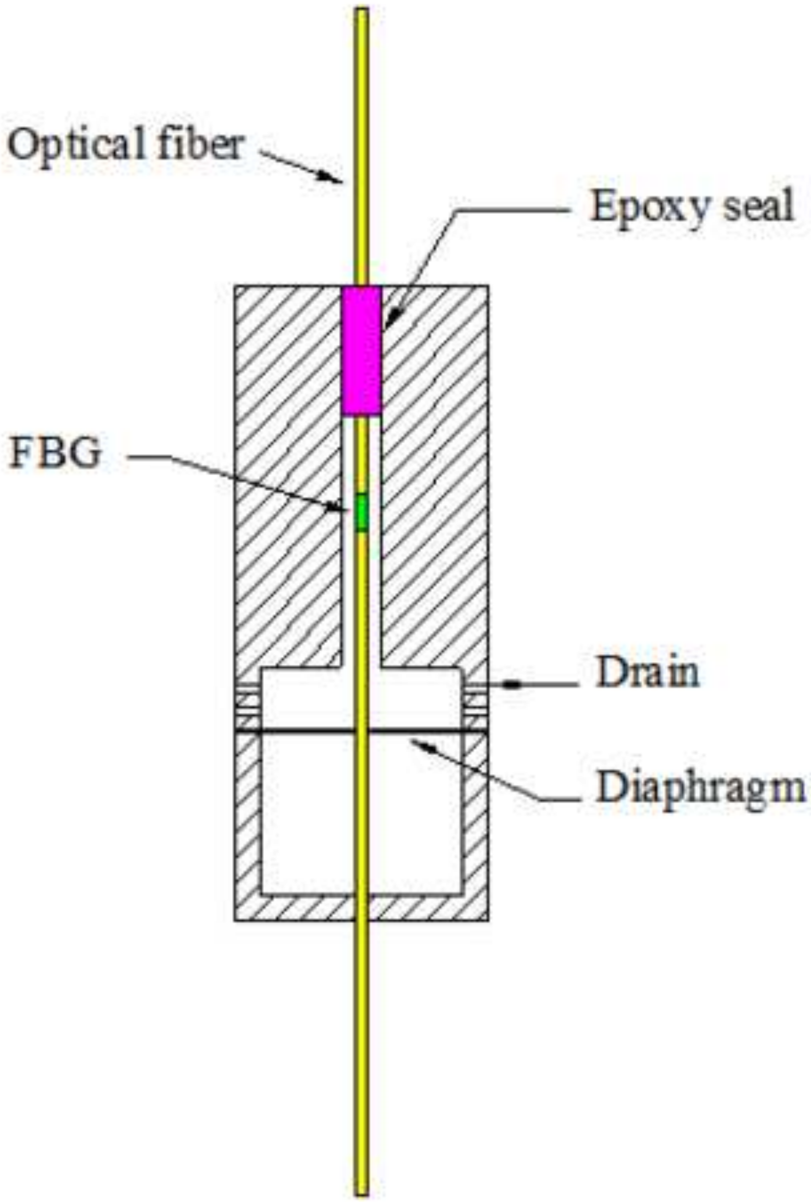

(Schematic view)

(Photograph)

Figure6

Click here to download high resolution image

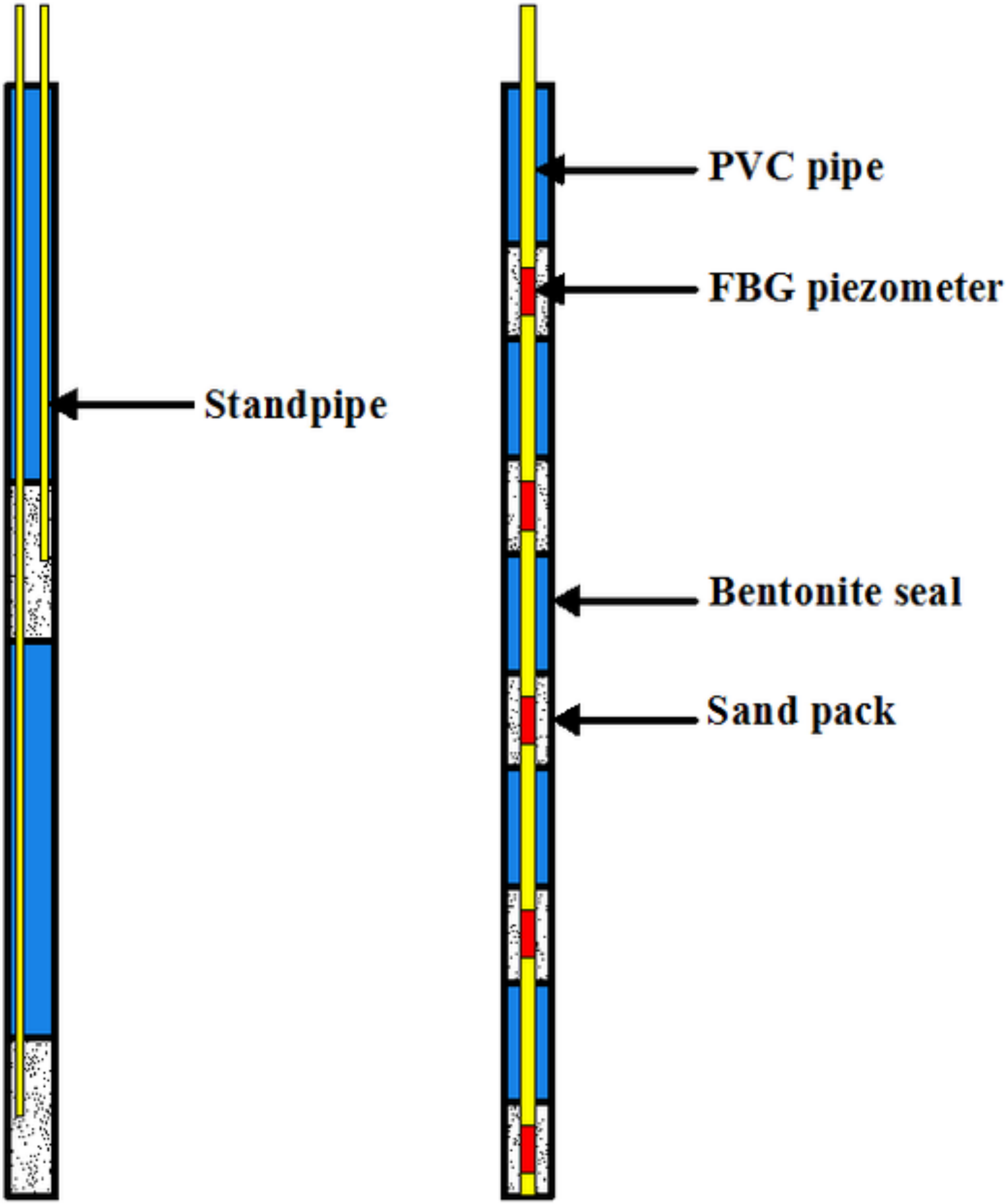

Figure7

Click here to download high resolution image

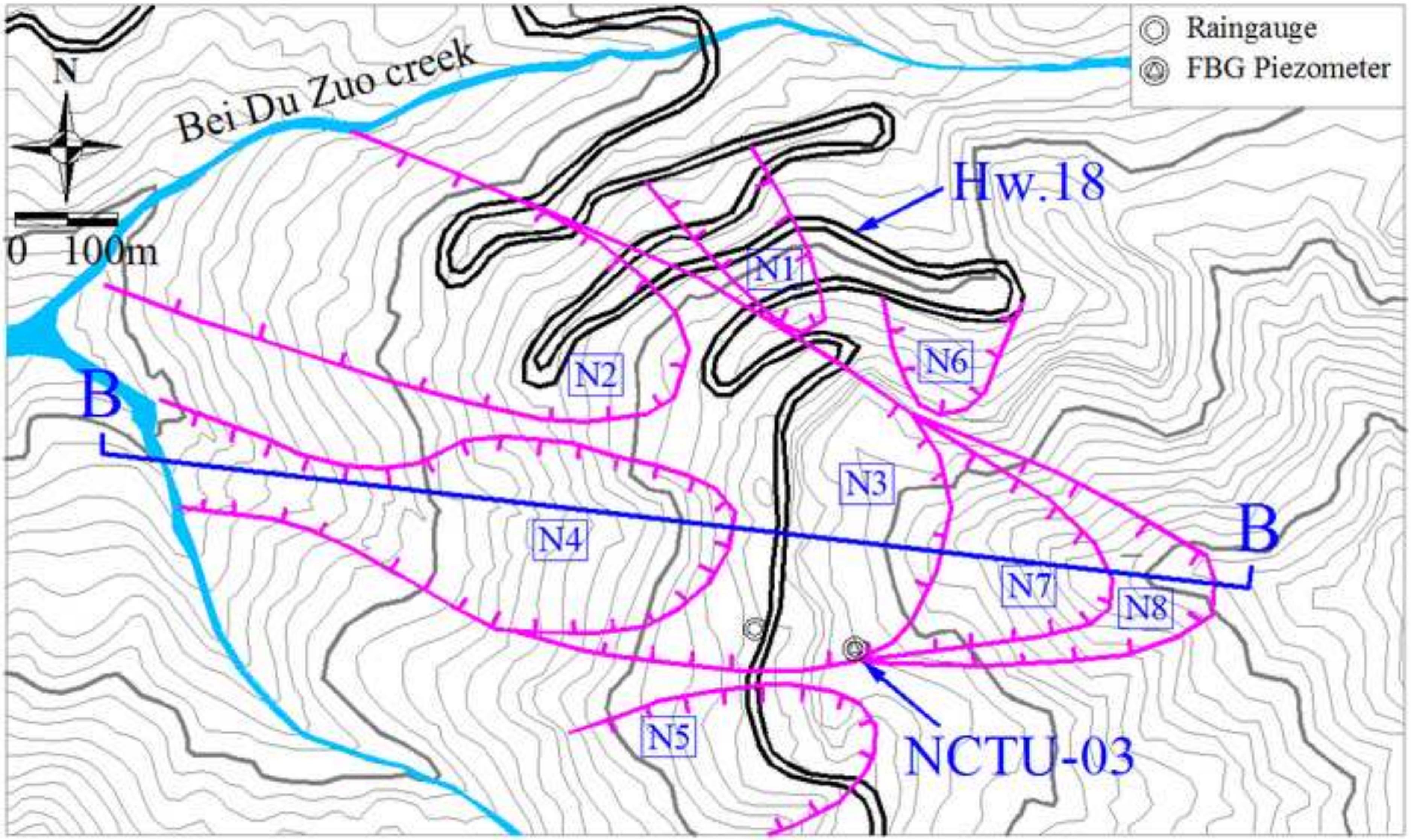

Figure8
Click here to download high resolution image

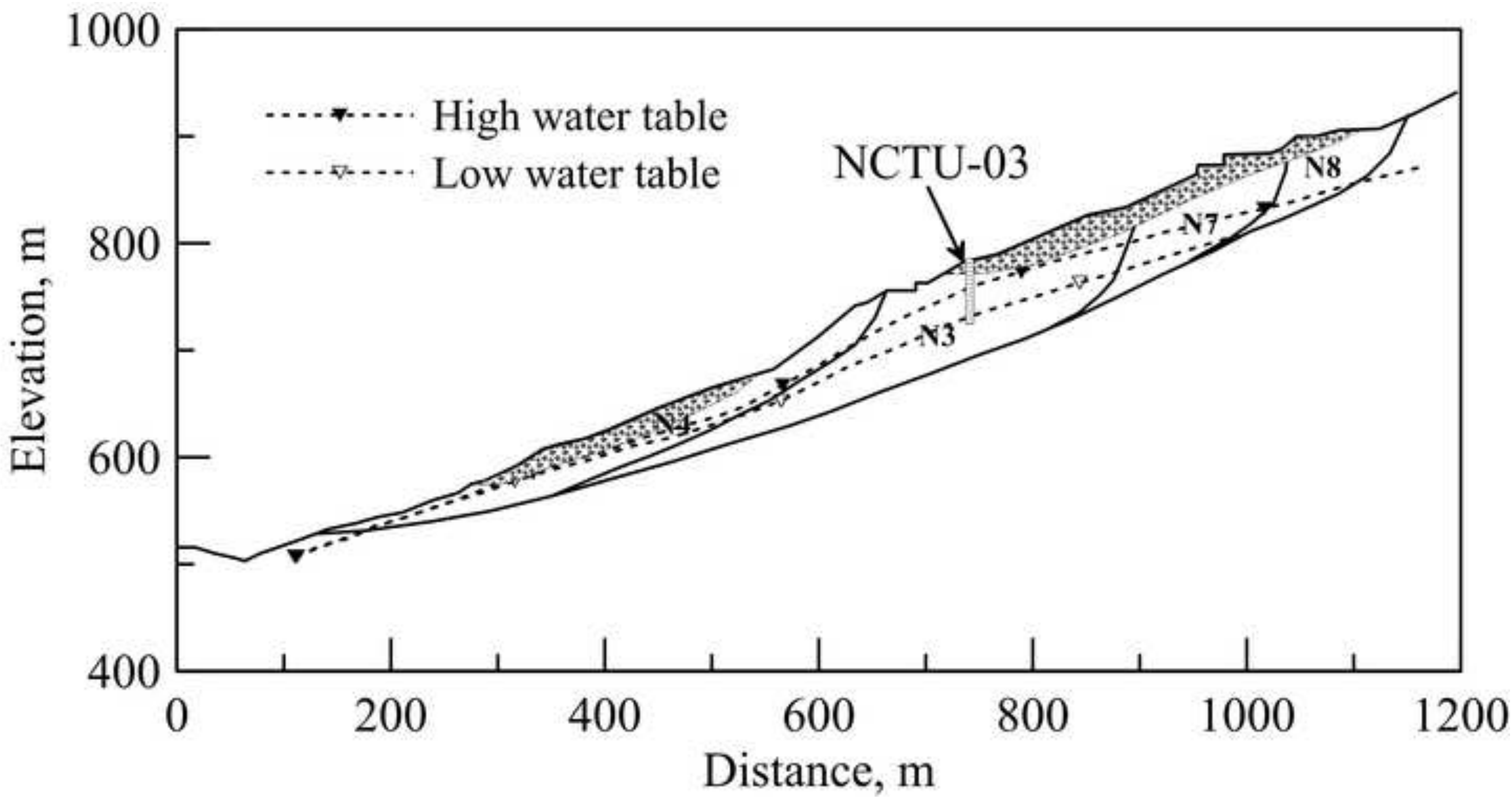

Figure9
Click here to download high resolution image

Figure10
Click here to download high resolution image

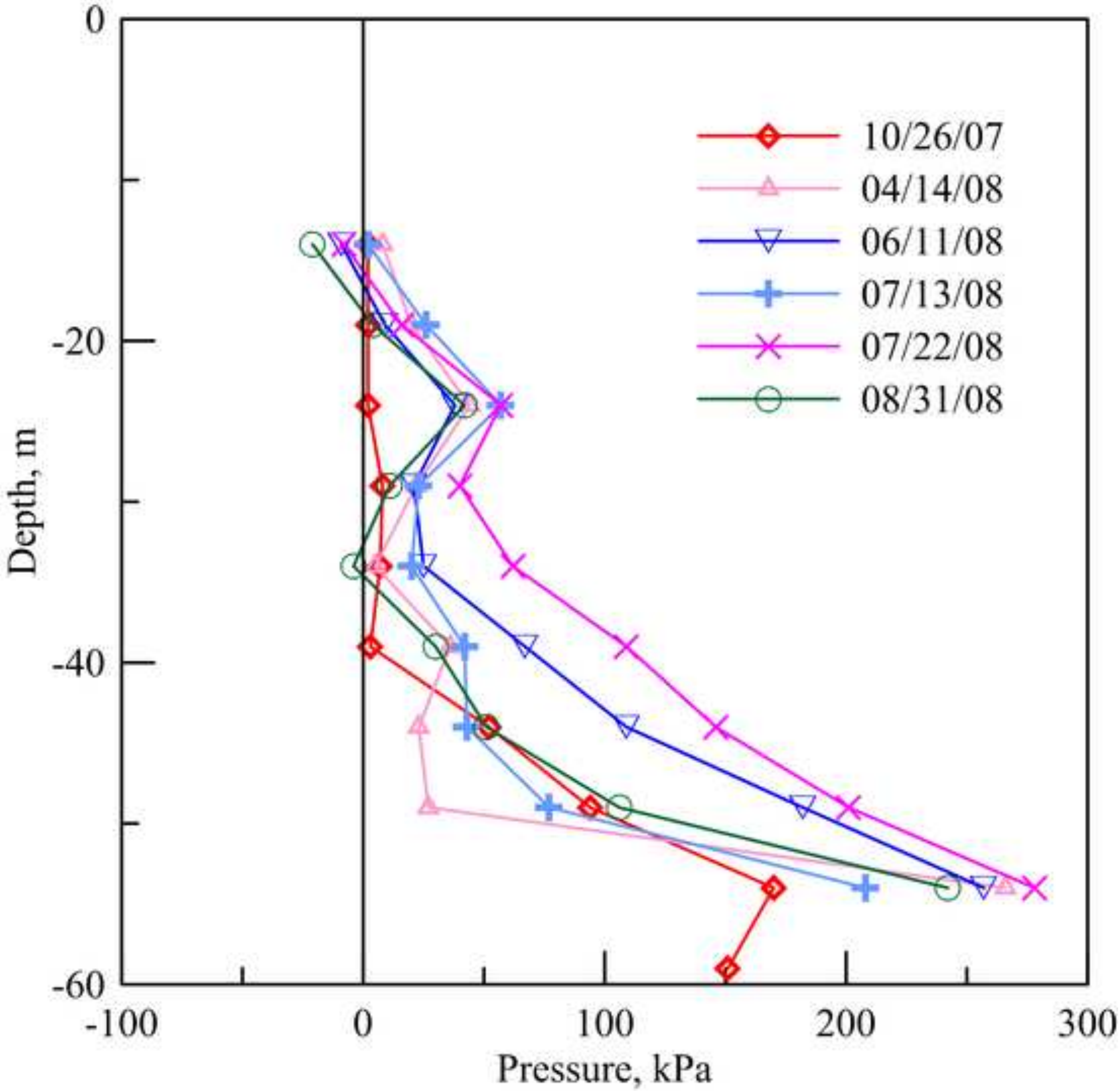

Figure11
Click here to download high resolution image

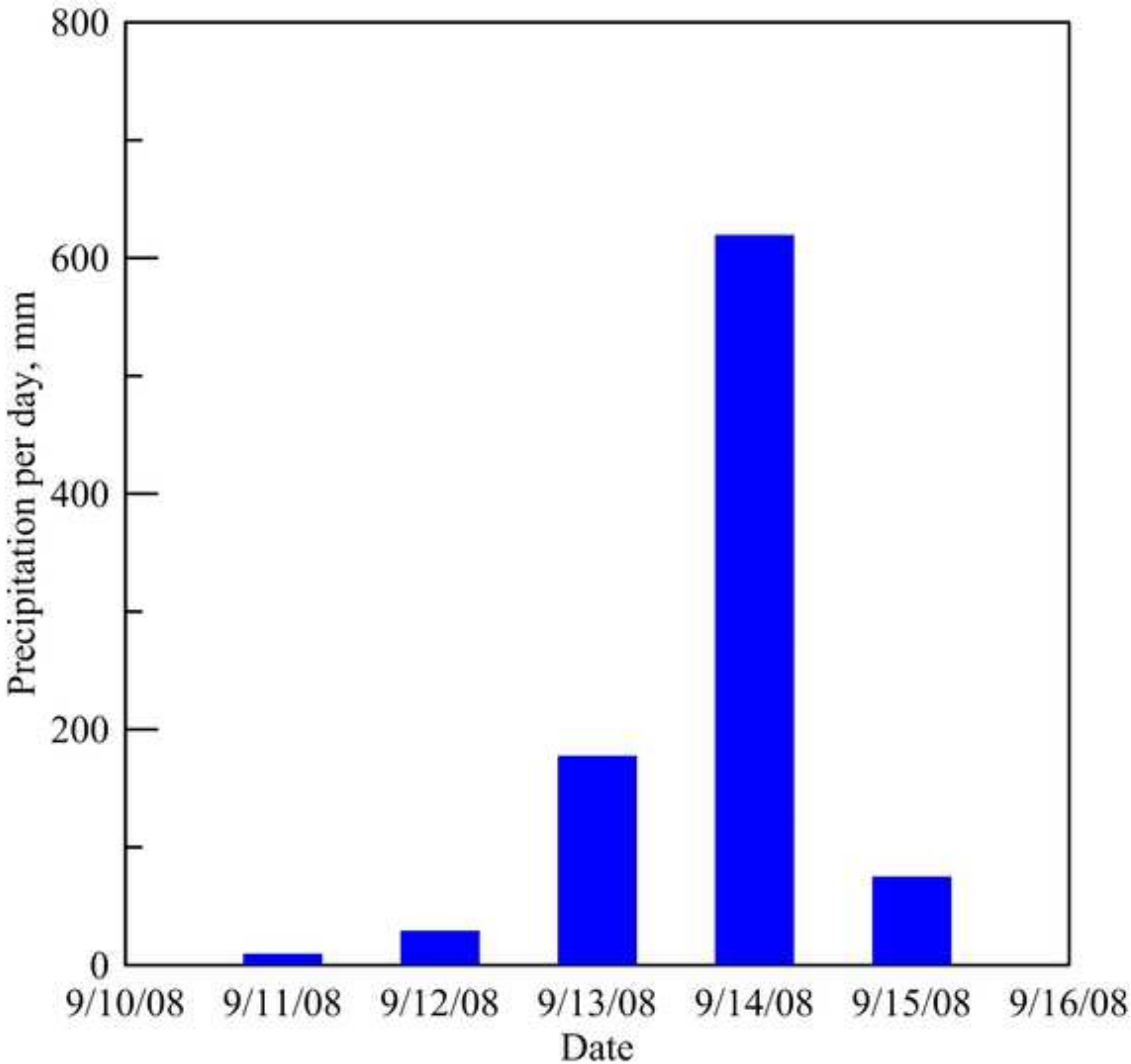

Figure12
Click here to download high resolution image

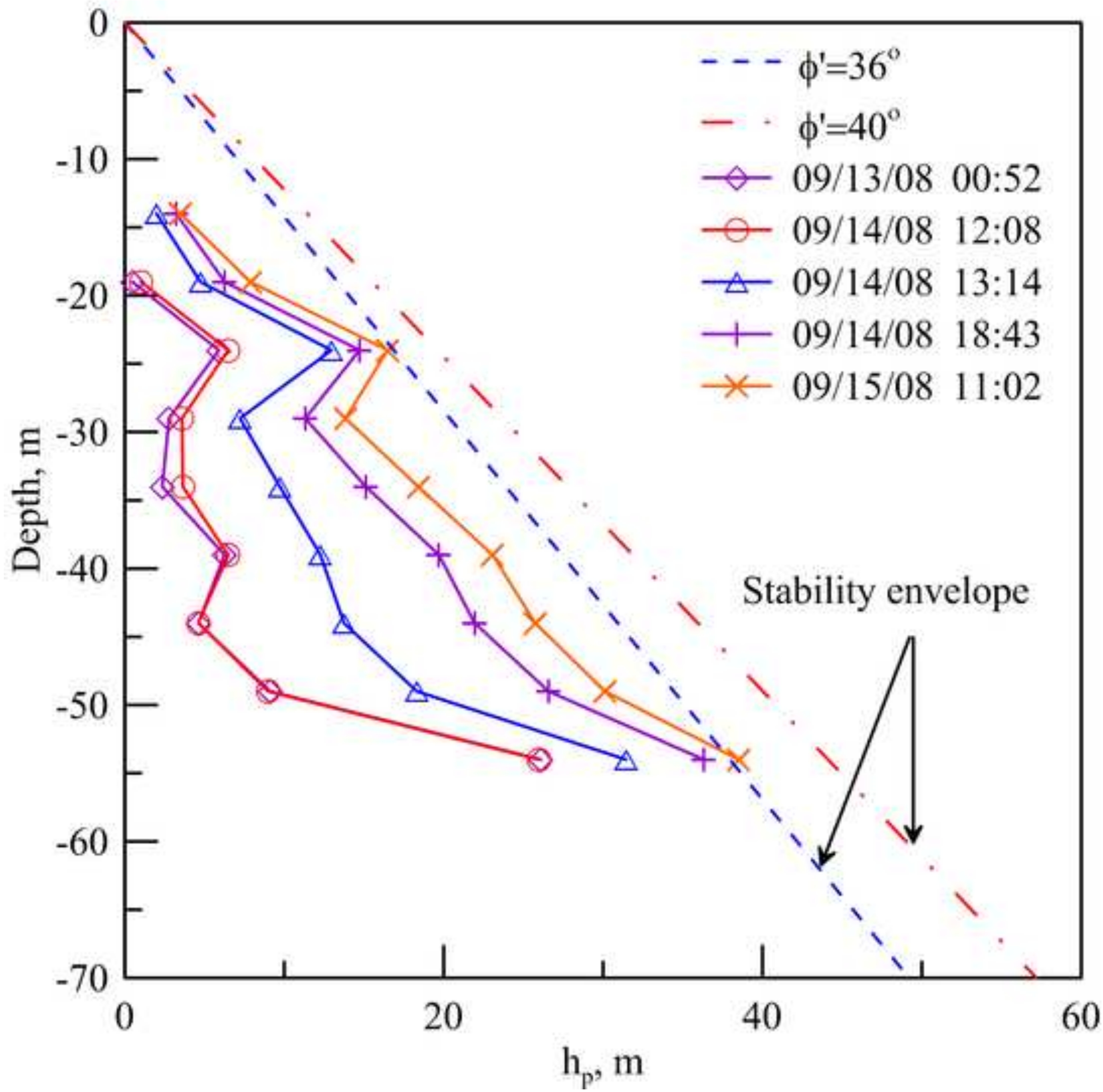

Figure13
Click here to download high resolution image

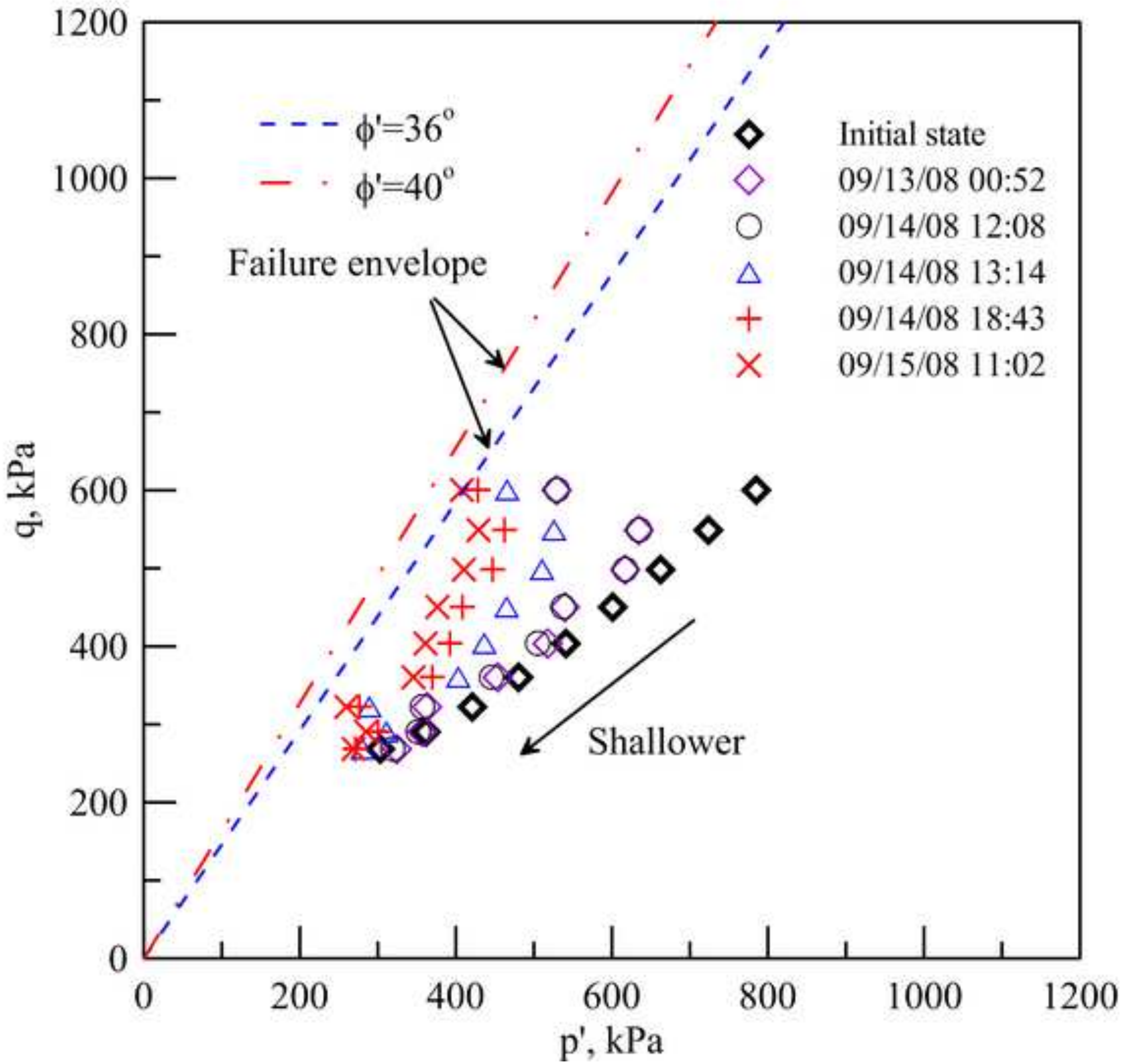

Figure14
Click here to download high resolution image

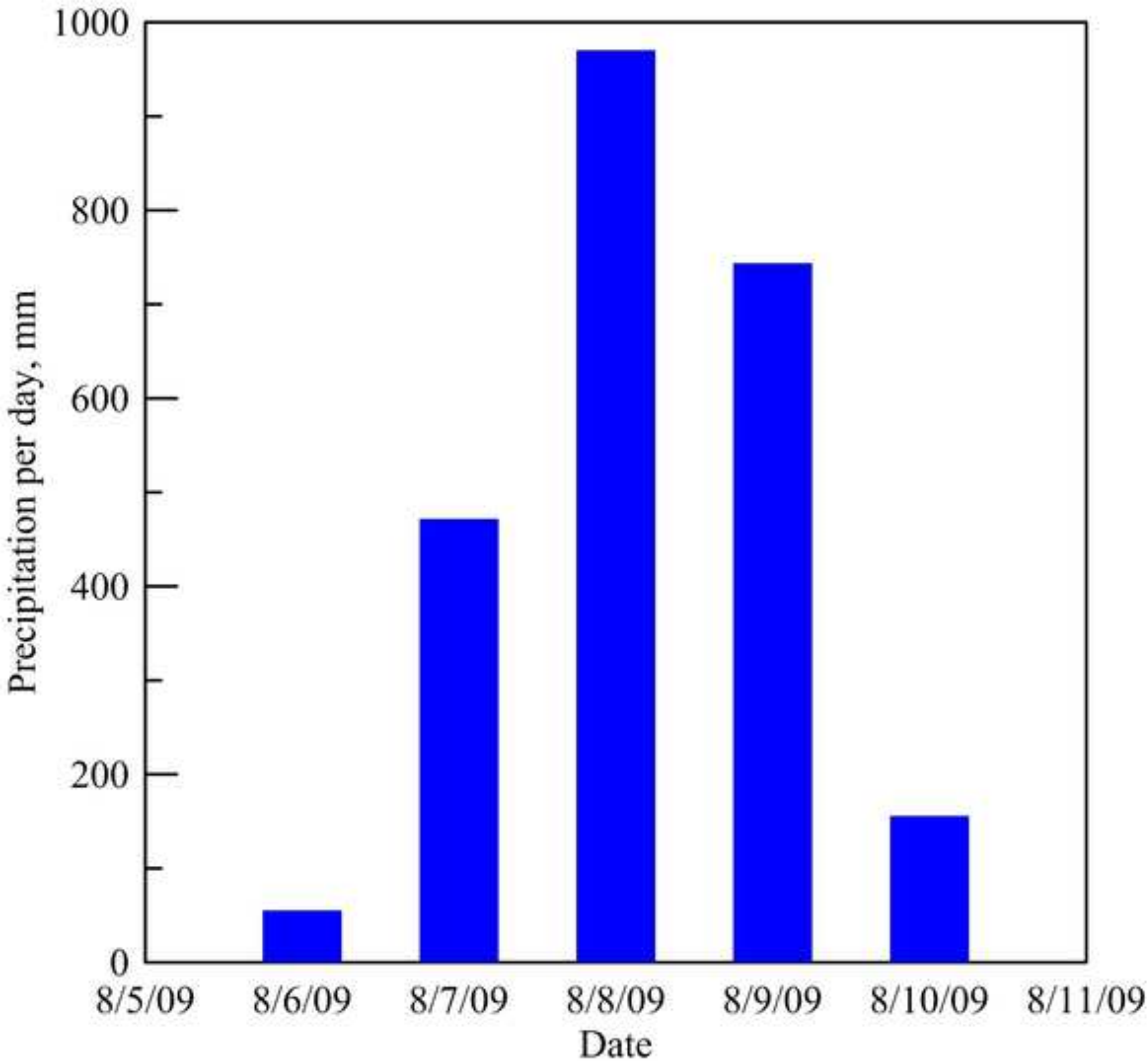

Figure15
Click here to download high resolution image

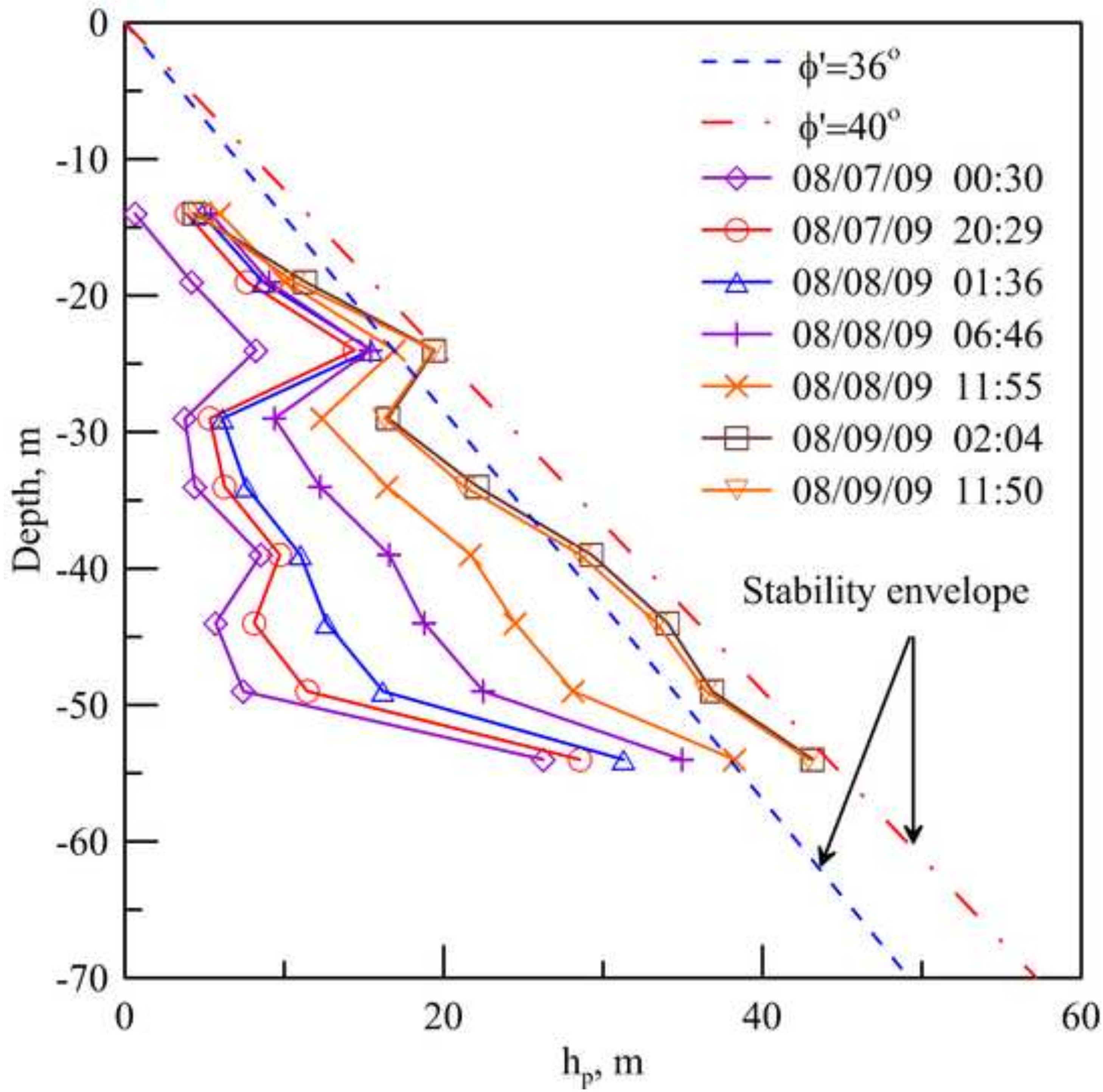

Figure16

Click here to download high resolution image

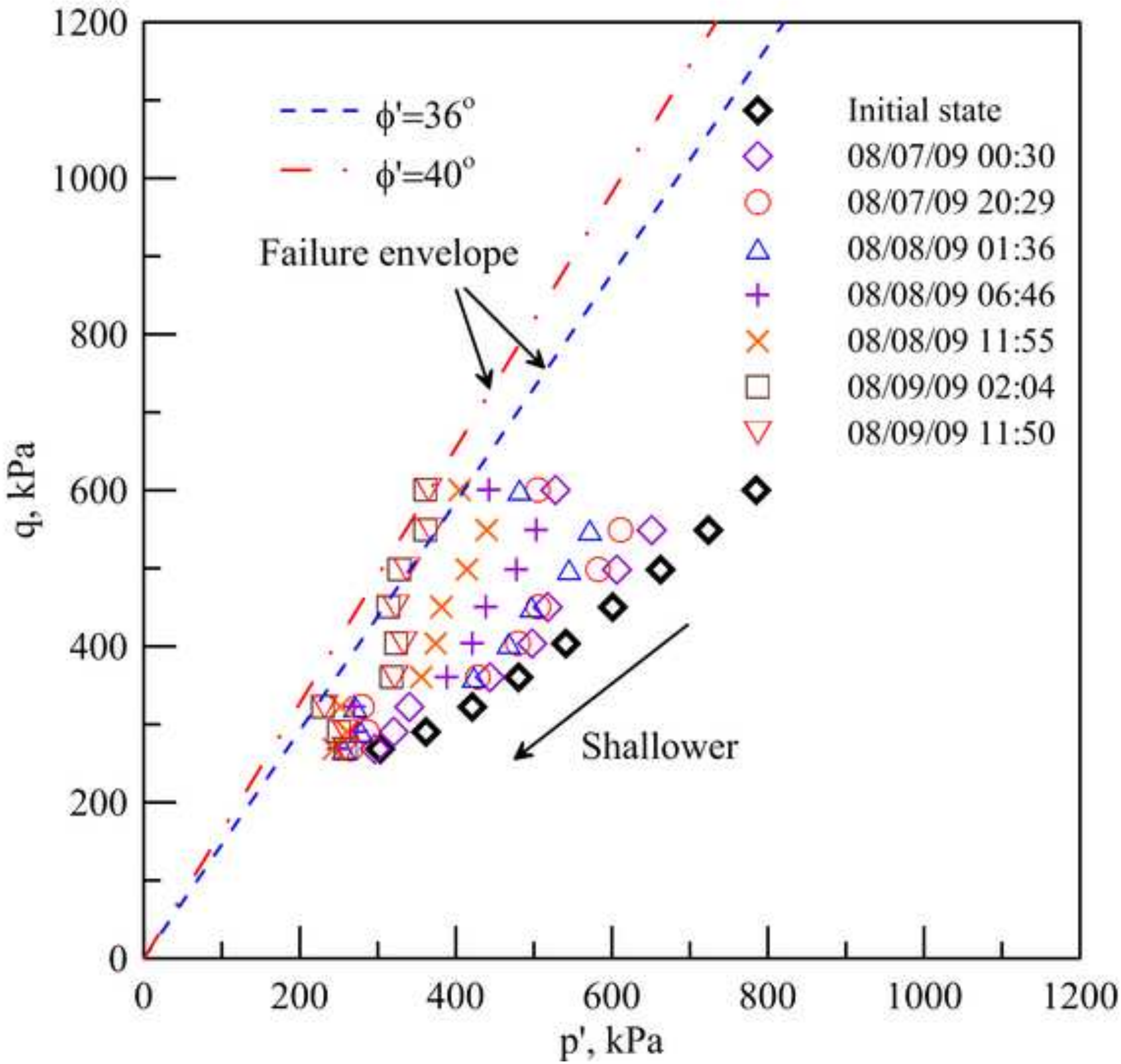

Figure17
Click here to download high resolution image

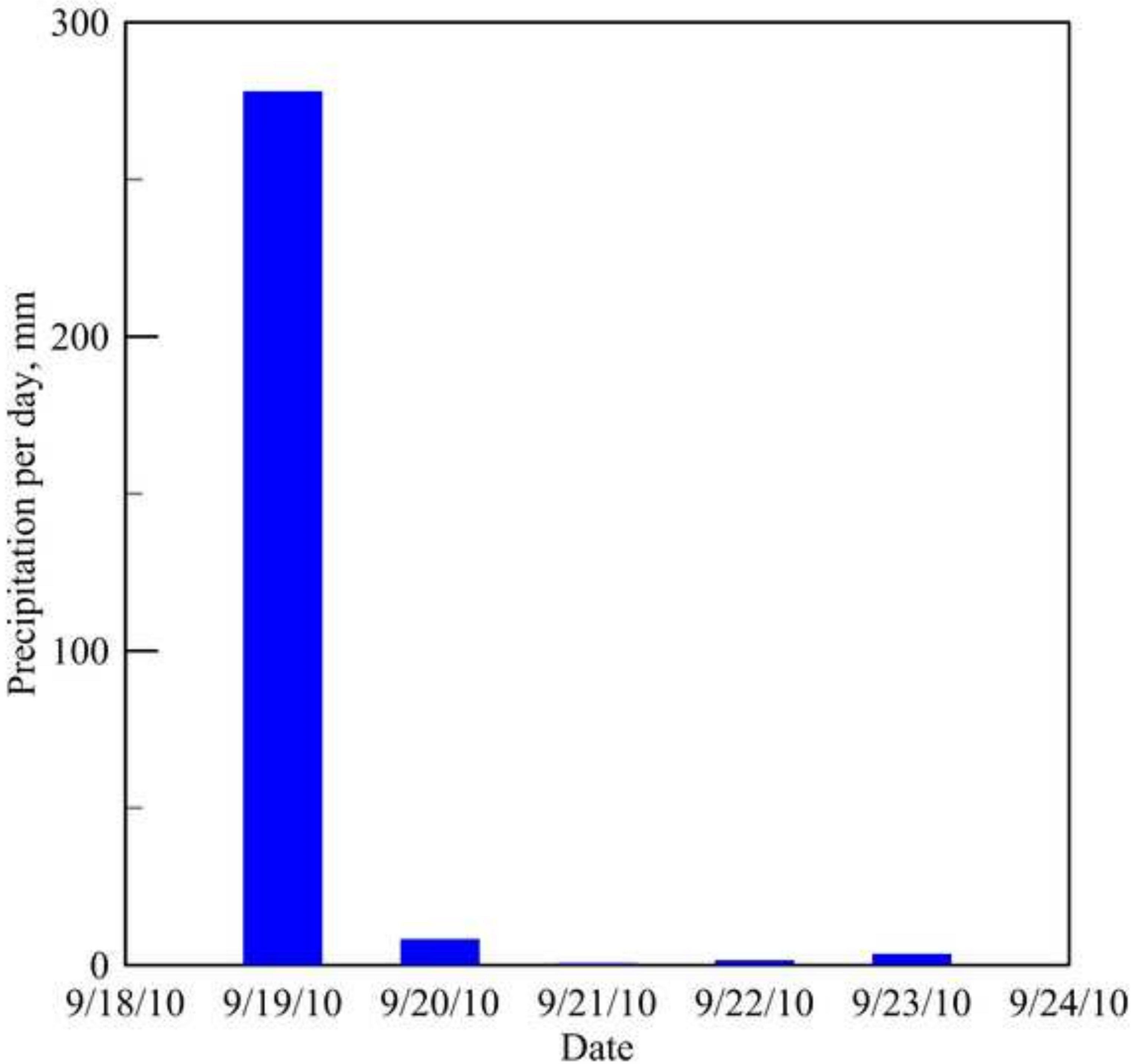

Figure18
Click here to download high resolution image

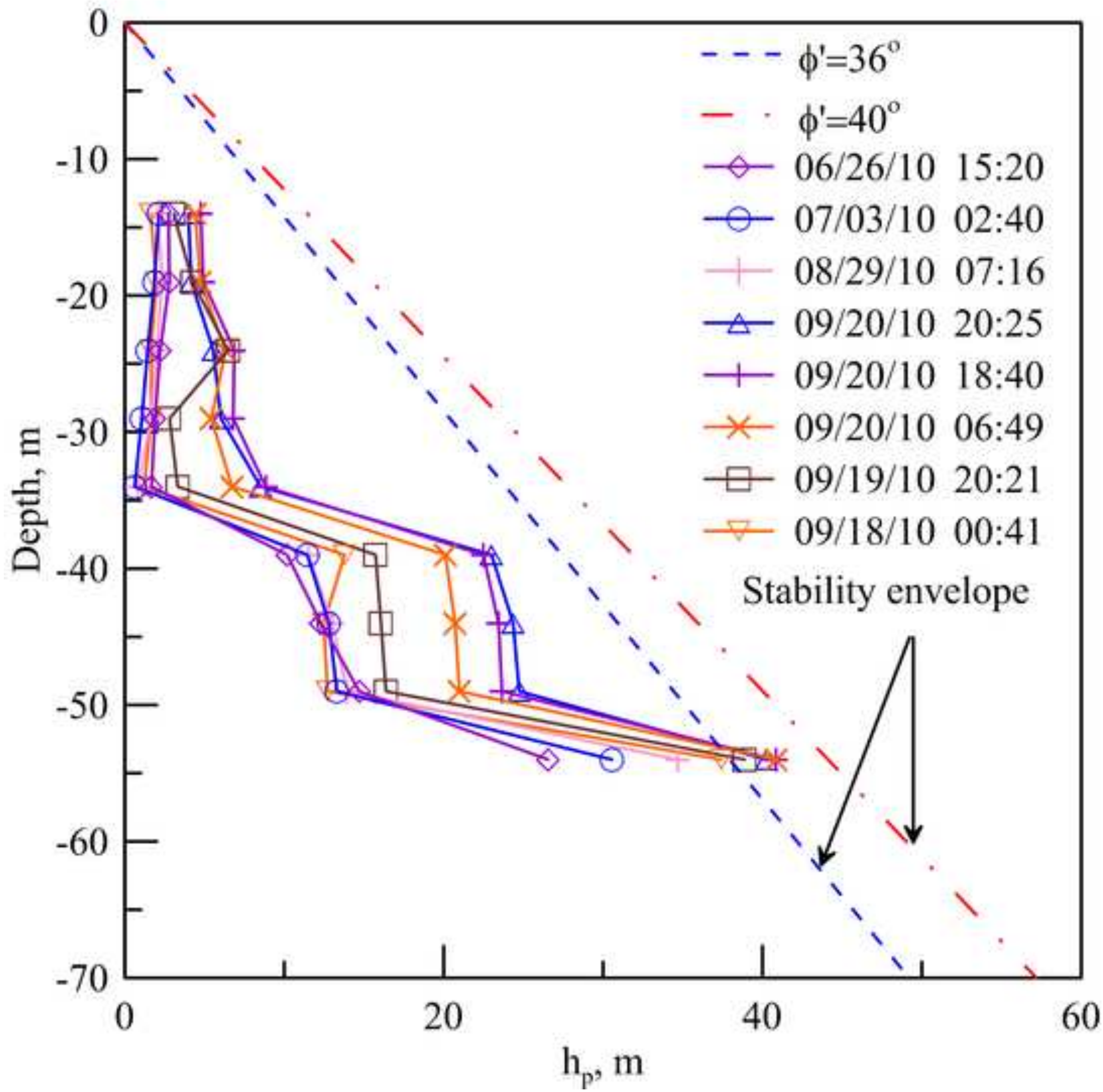

Figure19
Click here to download high resolution image

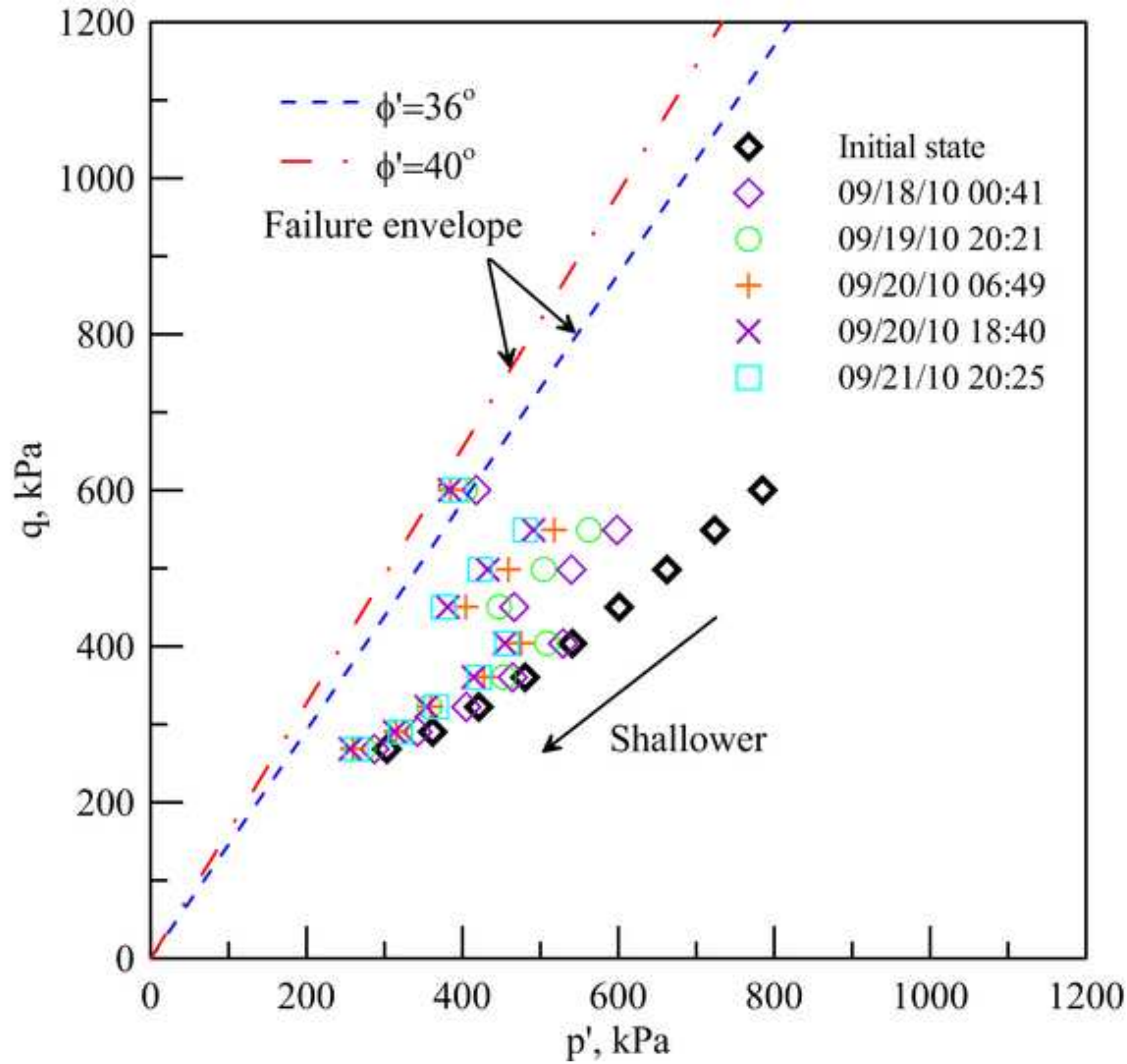

Table 1. Pressure head profiles used in method of slice analysis

Typhoon \ Depth	0m	14m	19m	24m	29m	34m	39m	44m	49m	54m
Sinlaku	0	3.46	7.81	16.42	13.78	18.35	22.96	25.64	30.03	38.45
Morakot	0	4.53	10.55	19.3	16.24	21.15	28.38	33.15	36.29	42.79
Fanapi	0	3.25	3.4	3.99	4.69	7.16	22.79	24.41	25.18	42.4

Table 2. Factors of safety from the analysis using the method of slices.

Friction angle \ Typhoon	Sinlaku	Morakot	Fanapi
36^{o}	0.97	0.92	0.80
40^{o}	1.12	1.07	0.92
45^{o}	1.34	1.27	1.09